remote sensing

MDPI

Article

Photophysiology and Spectroscopy of Sun and Shade Leaves of *Phragmites australis* and the Effect on Patches of Different Densities

Dimitris Stratoulias [1,2] and Viktor R. Tóth [3,*]

[1] Department for Management of Science and Technology Development, Ton Duc Thang University, Ho Chi Minh City, Vietnam; dimitris.stratoulias@tdtu.edu.vn

[2] Faculty of Applied Sciences, Ton Duc Thang University, Ho Chi Minh City, Vietnam

[3] Balaton Limnological Institute, Centre for Ecological Research, Tihany 8237, Hungary

* Correspondence: toth.viktor@okologia.mta.hu; Tel.: +36-87-448244; Fax: +36-87-482006

Received: 31 October 2019; Accepted: 31 December 2019; Published: 6 January 2020

Abstract: Remote sensing of vegetation has largely been revolving around the measurement of passive or active electromagnetic radiation of the top of the canopy. Nevertheless, plants hold a vertical structure and different processes and intensities take place within a plant organism depending on the environmental conditions. One of the main inputs for photosynthesis is photosynthetic active radiation (PAR) and a few studies have taken into account the effect of the qualitative and quantitative changes of the available PAR within the plants canopies. Mostly large plants (trees, shrubs) are affected by this phenomena, while signs of it could be observed in dense monocultures, too. Lake Balaton is a large lake with 12 km^2 dense reed stands, some of which have been suffering from reed die-back; consequently, the reed density and stress condition exhibit a vertical PAR variability within the canopy due to the structure and condition of the plants but also a horizontal variability attributed to the reedbed's heterogeneous density. In this study we investigate the expression of photosynthetic and spectroscopic parameters in different PAR conditions. We concentrate on chlorophyll fluorescence as this is an early-stage indicator of stress manifestation in plants. We first investigate how these parameters differ across leaf samples which are exposed to a higher degree of PAR variability due to their vertical position in the reed culm (sun and shade leaves). In the second part, we concentrate on how the same parameters exhibit in reed patches of different densities. We then look into hyperspectral regions through graphs of coefficient of determination and associate the former with the physiological parameters. We report on the large variability found from measurements taken at different parts of the canopy and the association with spectral regions in the visible and near-infrared domain. We find that at low irradiance plants increase their acclimation to low light conditions. Plant density at *Phragmites* stands affects the vertical light attenuation and consequently the photophysiological response of basal leaves. Moreover, the hyperspectral response from the sun and shade leaves has been found to differ; charts of the coefficient of determination indicate that the spectral region around the red-edge inflection point for each case of sun and shade leaves correlate strongly with ETR_{max} and α. When analysing the data cumulatively, independent of their vertical position within the stand, we found correlations of $R^2 = 0.65$ (band combination 696 and 651) and $R^2 = 0.61$ (band combination 636 and 642) for the ETR_{max} and α, respectively.

Keywords: reed; spectroscopy; chlorophyll fluorescence; photosynthesis; foliar density; PAR

1. Introduction

Light is the primary source of energy for plants, affecting their growth, development and structure in both terrestrial and aquatic settings, and creating strong selection pressure through its variability [1–3].

Adequate response to light is of central importance for plants since either a suboptimal or an excessive amount of it could result in significant decrease of its fitness; therefore, low-light and high-light adaptation processes in plants have been discovered and studied [4,5]. It has been observed since a long time ago that plants which grow under a shaded environment and plants which grow under high light intensities exhibit distinguished photosynthetic activity and efficiency [6]; moreover, individual leaves, as a functional unit of biomass production, are utilising and being affected by the intensity and spectral composition of the sunlight. This successful adaptation to different light intensities at the apical and basal parts of the plant is possible due to greater flexibility of foliar responses and, thus, more effective light capture. Eventually, the constant competition for light harvesting results to an additional increase in spatial and temporal foliar variability that alters the architecture of individual plants [3,7]. Consequently, for instance, Lichtenthaler et al. [8] studied the pigment composition and photosynthetic activity of deciduous and coniferous plants and concluded that the sun leaves of all tree species were thicker, with lower specific leaf area and water content and higher total chlorophyll a + b and carotenoid content per leaf area unit compared to the shade leaves. Schultz [9], in a study measuring the reflectance of grapevine (*Vitis vinifera* L.) leaves, reports that reflectance was highest at the beginning of the season for apical leaves and at the end of the season for basal senescent leaves, evidencing the temporal changes occurring. In another old study, Gausman [10] measured total defuse reflectance over the 500–750 nm spectral window on Valencia orange (*Citrus sinensis* (L.) Osbeck) leaves and indicated that there are considerable differences between the shade and sun leaves of the specific species. For a review on the changes induced by conditions of sun (high light) and shade (low light) on the process of photosynthesis, the reader is directed to Mathur et al. [11].

A prime example of species which demonstrates a wide variability of available photosynthetically active radiation (PAR) in its structure is that of common reed (*Phragmites australis* (Cav.) Trin. ex Steudel). *Phragmites* is a widespread tall rhizomatous perennial grass [12] growing in wetland environments [13]. It typically forms dense reedbeds which allow only a fraction of the available PAR to reach the basal parts of the plant, hence, its architecture inherits differing conditions in the vertical PAR availability. Moreover, different patches of reedbed, depending on the environmental conditions, may grow in different densities, diversifying the horizontal PAR availability as well.

On this note, since the beginning of the 1960s, a decline of the reed area, especially in the waterward side of the stands, has been observed in several parts of Europe [14,15]. This phenomenon, known as reed die-back syndrome, was first scientifically documented in 1951 (as cited by Ostendorp [16]) and scientific interest has been brought up. Reed die-back is manifested through reduced plant height, weaker culms, abnormal rhizomes, formation of clumps [17], gradual thinning, natural degeneration and retreat from relatively deep water [15]. Consequently, reed die-back is inducing spatial fragmentation and, therefore, altering the density, the natural horizontal (zonation) and vertical structure of the reed stand.

Photosynthesis is the plant's prime process of light harvesting; incident solar energy is absorbed by leaves and through a system of energy transfers is converted to chemical energy that sustains the organism's functions and eventually leads to biomass accumulation. The first step of this energy transfer (the absorption of light) is performed by photosystems of autotrophs that regulate not only the absorption, but also the dissipation of the unused energy within the photosynthetic organ. One of the tools for assessing the dynamic changes occurring in the photosystems is chlorophyll fluorescence [18,19]. Emphasis on research on chlorophyll fluorescence and photosynthesis has increased the last decades, indicated by the steep increase from 1990 onwards of the number of publications relating to the keywords aforementioned [20].

Remote sensing has been long used in vegetation studies in a variety of applications and, currently, an abundance of data and tools are available to ecologists [21,22]. For instance, hyperspectral data is essentially the most detailed representation of the spectrum and, hence, can provide a wealth of information at canopy and foliar levels likewise. However, in the context of vegetation monitoring, the majority of the spectral information, which is materialized as vegetation indices, is constructed to

relate to vegetation traits other than photosynthesis; for instance, chlorophyll content has been a feature suggested to be approximated by the ratio of reflectances at the red-edge wavelengths at 750 nm and 710 nm (i.e., R750/R710) by Zarco-Tejada et al. [23], R750/R550 and R750/R700 by Gitelson and Merzlyak [24] and the empirical indices modified Normalized Difference Vegetation Index (mNDVI) [25], the Plant Senescence Reflectance Index (PSRI) [26] and the Structure Insensitive Pigment Index (SIPI) [27], just to name a few. Other traits have also been related, such as xanthophyll with the Photochemical Reflectance Index (PRI) [28]. Another variable frequently attempted to relate to spectroscopic information is the poor performance of the plant in terms of the photo-efficiency, which is generically named as "stress". In any case, it is not a mainstream procedure that the physiology/photosynthetic process of the plant is directly associated to the spectral information; despite the fact that both chlorophyll fluorescence and remote sensing are quite established techniques, only lately this field is gaining attention (e.g., [22,29–32]). This has mainly taken place in the context of passive remote sensing targeting the analysis of sun induced fluorescence features (e.g., [33]), which are a precursor sign of plant stress and reduced photosynthetic activity. Narrow-band PRI has been proposed to assess PS II Light-Use Efficiency (LUE) [34] and suggested as a good proxy for photosynthetic efficiency at different spatial and temporal scales [35]; however, PRI may vary and depends on environmental conditions such as nutrients, water status or temperature [36]. Other studies have reported strong correlation of popular empirical indices, such as the the Normalized Difference Vegetation Index (NDVI), with canopy photosynthesis (e.g., [37,38]). In a recent study Dechant et al. [39] suggest that nitrogen content is the dominant mechanism through which photosynthesis is related to leaf reflectance spectra; they also argue that their method is applicable to many tree species and both sun and shade leaves. Finally, in the context of foliar and plant density, another important application of earth observation is mapping the density variability with remote sensing images. The explanation of this variability might be related to spectral indices. This spatio-temporal exhibition is especially suitable for the study of emergent macrophytes.

This papers studies the expression of the photosynthetic and spectroscopic parameters in different PAR conditions; more specifically, we focus on two aspects. First, we measure certain physiological and hyperspectral parameters from *Phragmites* leaf samples, which are exposed to a different degree of available PAR due to their vertical position in the reed culm (sun and shade leaves) and we investigate if and how the parameters differ and associate with each other. In the second part, we look into the exhibition of these parameters on leaves grown in reed patches of different densities.

2. Materials and Methods

2.1. Study Site

Lake Balaton is a large (596 km^2) and relatively shallow (average water depth 3.5 m) freshwater lake located in Central Europe. Extended and continuous populations of helophytic perennial plants at the littoral zone of the lake form reed stands scattered along 112 km of the 240 km of the total shoreline [40,41]. The reed stands cover cumulatively an area of approximately 16 km^2 with the majority of it (73%—12 km^2) encountered at the northern part of the shore. The steep windward northern shore's sediment consists of dolomite limestone, while the shallow southern shore is dominated by sandy sediment. On the northern shore of the lake the average and maximum depth of water that reed stand can be found is 1.5 m and 2.4 m respectively, while on the southern shore the average depth on the waterward side of reed stands is 1 m [40,41]

Lake Balaton has received significant scientific attention due to the reed die-back phenomenon observed (e.g., [40–43]), the macrophytic traits and species mapping (e.g., [44–47]) and the dynamic trophic gradient of the water (e.g., [48,49]). The field data for this study were collected at the Kerekedi bay, an oligo-mesotrophic bay at the easternmost basin of Lake Balaton situated at the geographic coordinates 46°58′2.84′′ N, 17°55′4.34′′ E (Figure 1). The main species encountered there are *Phragmites australis*, *Carex* sp., *Typha angustifolia*, *Typha latifolia* and *Bolboschoenus* sp. The survey took place under

clear sky conditions between 10:00 and 13:00 local time (Central European Time) on 14–15 August 2012. This period falls within the peak of the vegetation growing and all species are at full growth.

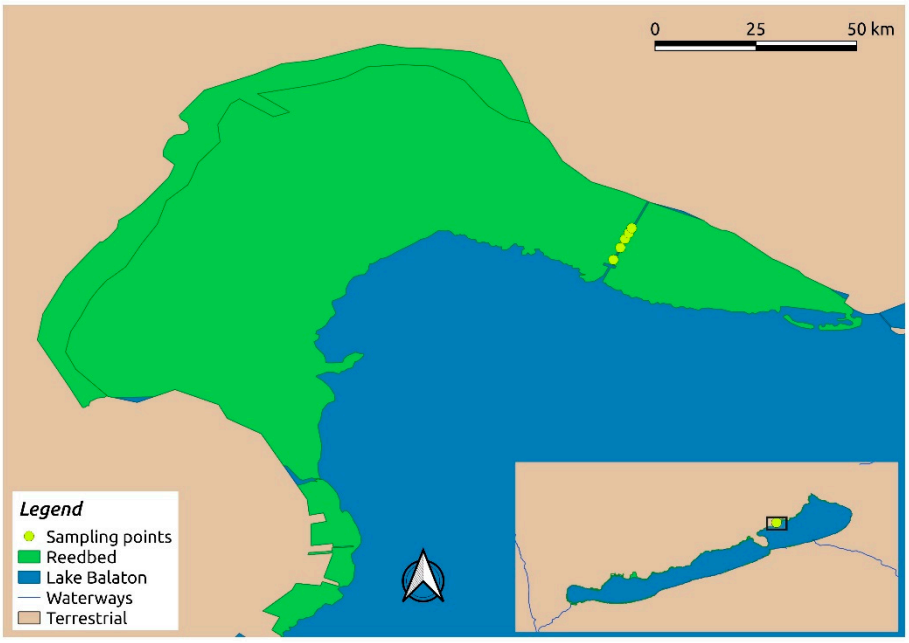

Figure 1. Map of the study area in Lake Balaton (inset) and field sampling points' location in the Kerekedi Bay (main).

2.2. Data Survey

Chlorophyll fluorescence and spectroradiometric measurements were collected along a perpendicular-to-the-shore transect. Two types of measurements were performed on *Phragmites* plants on-site. Firstly, the largest fully emerged green apical and the largest intact green basal leaves, of approximately 4 m high plants in a dense (>80 plants m^{-2}) and non-degrading stand, were selected. These leaves are referred to thereafter as the sun (youngest, mature, apical) and shade (oldest, mature, basal, green) leaves, respectively. Second, photophysiological parameters of oldest, mature, basal, still green leaves of *Phragmites* were determined in reed patches of varying density. The plant density was estimated from a photograph captured at ground level (water or soil) from an upward looking camera.

2.2.1. Photophysiological Measurements

The light response curves (i.e., the electron transport rate (ETR) of photosystem II (PSII) as a function of PAR intensity) of leaves were measured with a pulse amplitude modulated chlorophyll fluorometer (PAM-2500, Heinz Walz GmbH, Effeltrich, Germany). A 20 min dark adaptation period was applied in the beginning of the routine and the same actinic light was used for both sun and shade leaves. First, the fluorescence values were detected for a dark adapted leaf with a pulse of a saturated light (630 nm, intensity 3000 µmol m^{-2} s^{-1}). Thereafter, the leaves were exposed to 11 actinic lights (at 5, 9, 67, 104, 144, 201, 274, 366, 477, 622 and 788 µmol m^{-2} s^{-1} intensity, see Figure 2) at 630 nm wavelength with a duration of 15 s; subsequently, the fluorescence values were measured after each illumination step with a new pulse of saturated light (3000 µmol m^{-2} s^{-1}). During this process the minimal (F_0) and maximal (F_m) fluorescence yield of a dark-adapted leaf, as well as the fluorescence yield (F), maximal fluorescence yield (F_m') during saturation pulse and minimal fluorescence yield (F_0') of a pre-illuminated sample were determined. The equipment calculated other parameters using these fluorescence yields (Table 1).

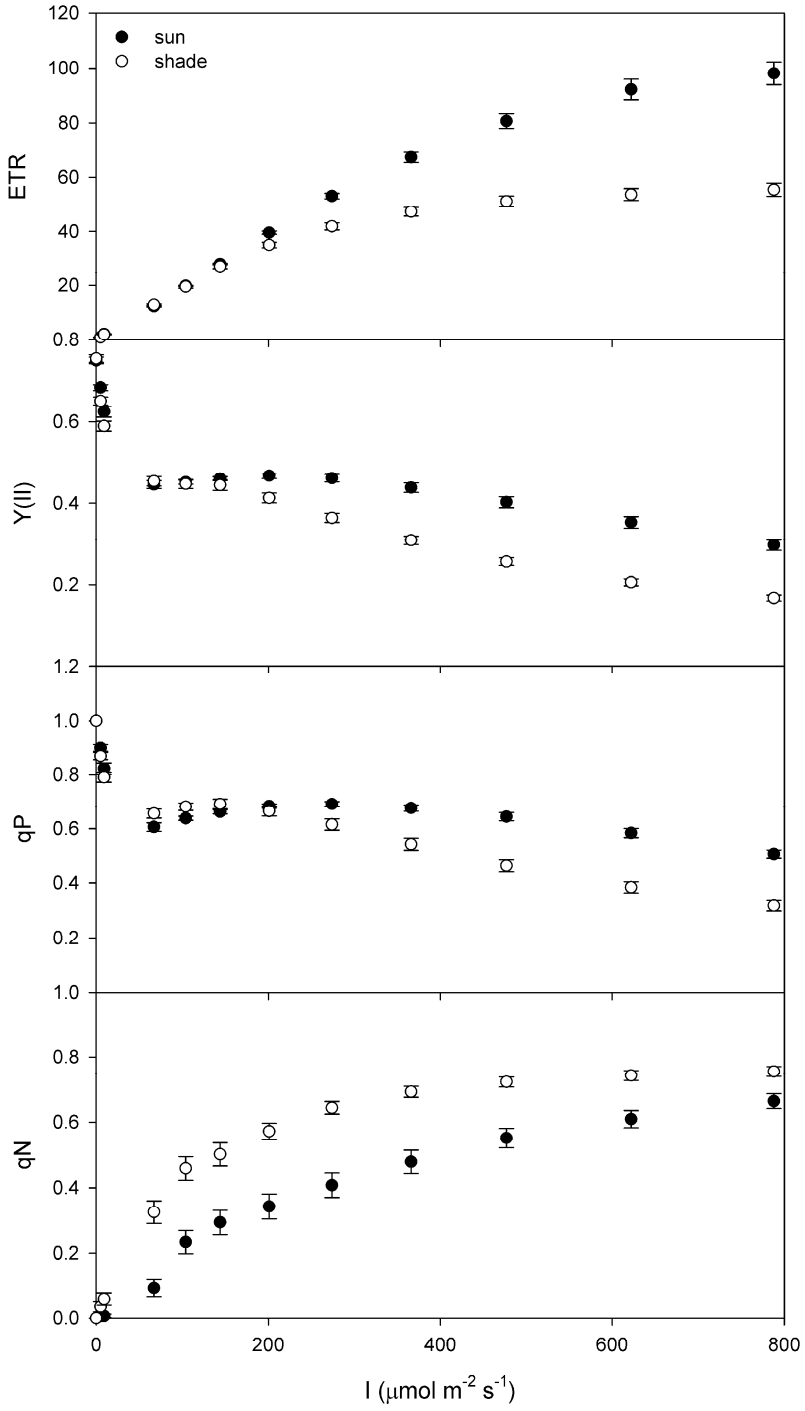

Figure 2. Light curve of photophysiological parameters of the sun (black circles) and shade (open circles) leaves of *Phragmites australis*. The ± Standard Deviation (SD) (n = 15) is also indicated for each measurement.

Table 1. Fluorescence parameters calculated from PAM fluorometry. The equations contain the minimum (F_0) and the maximum (F_m) fluorescence yields, the apparent (F_s) and maximum (F_m') values of fluorescence, the irradiance value (I) and the empirical absorption factor (AF = 0.84). For more information the reader is directed to the cited literature.

Parameter	Name	Equation
qP	photochemical quenching	$(F_m' - F)/(F_m' - F_0')$
qN	non-photochemical quenching	$1 - (F_m' - F_0')/(F_m - F_0)$
Y(II)	quantum yield of PSII	$(F_m' - F)/(F_m')$
ETR	electron transport rate	$(F_m' - F)/(F_m')\cdot I\cdot AF\cdot 0.5$

2.2.2. Spectroradiometric Measurements

The reflectance values of sun and shade *Phragmites* leaves were recorded using a hand-held ASD portable FieldSpec 2 spectroradiometer (Analytical Spectral Devices Inc., Boulder, Colorado, USA). The instrument records radiation intensity in 750 consecutive narrow-bands between 325 nm and 1075 nm with a spectral resolution of less than 3 nm at 700 nm. Leaf reflectance values were acquired with the ASD leaf clip attached to the device with an optical fibre. The source of light was integrated in the leaf clip and the black reference panel on the opposing side was used to calibrate the instrument in order to convert the recorded radiance values to reflectance. For each leaf sample 10 measurements were recorded from the same point at 544 ms integration time and then averaged. Three positions of the leaf were identified (i.e., next to the stem, middle of the leaf and upper third of the leaf) which did not yield any statistical differences in reflectance values (data not shown here), therefore, the measurements from the upper third of the leaf blade were used.

2.3. Data Analysis

The mean values of the photophysiological properties of sun and shade leaves were compared on the basis of the Student's *t*-test and the Mann-Whitney Rank Sum test. The measurements were taken from the same position as the hyperspectral measurements aforementioned. Parameters were correlated with Pearson and Spearman Rank Order correlations. The light response data were fitted with an exponentially saturating curve [50] with the method of the least squares applied on exponential rise; subsequently, the maximum ETR (ETR_{max}), theoretical saturation light intensity (I_k) and the maximum quantum yield for whole chain electron transport at low radiation (α) were retrieved [18]. The analysis was performed in the statistical software R version 2.15.3 [51]. Sigma Plot v 12.5 (Systat Software Inc., San Jose, California, USA) was used for the curve fitting and the production of the graphics.

The hyperspectral data were first exported using the software ViewSpec Pro 6.0 (Analytical Spectral Devices Inc., Boulder, Colorado, USA) and the marginal wavelengths at 325–400 nm and 1000–1075 nm from all spectra were removed as they contained a high level of noise. Subsequently, the spectra were divided in shade and sun samples according to the collection protocol and the curve of the mean and standard deviation of the reflectance value for each group was plotted. Moreover, the first derivative of the mean value was explored and the wavelength of the inflection point (λ_p) was used as the measure of the position of the red-edge reflectance critical value. Thereafter, the exhaustive combination of spectral indices for all spectral bands, as in similar studies (e.g., [22,52,53]), was calculated based on the mathematical formula:

$$NDSI(i,j) = (Ri - Rj)/(Ri + Rj)$$

where NDSI is the Normalised Difference Spectral Index (NDSI) and Ri and Rj are the reflectance values for bands i and j, respectively. Three physiological parameters were correlated with the NDSI, namely α, ETRmax and I_k. For each parameter and each NDSI combination, we calculated the coefficient of determination (R^2) and the corresponding significance level (p) assuming a linear relationship for the n pair of measurements of hyperspectrum and physiological parameter recorded in each experimental

setup. The results were visualized using raster maps of the coefficient of determination. The R^2 values corresponding to spectral pairs yielding $p > 0.05$ (which is deemed statistically insignificant) were masked out to highlight only the statistically significant regions, based on which the results were interpreted. The spectral regions which yields the highest R^2 between the NDSIi,j and the parameter under study can then be identified. Moreover, several popular empirical indices were extracted as presented in Table 2. For the hyperspectral calculations, the R programming language was used as well [51].

Table 2. Empirical vegetation indices extracted from the hyperspectral data collected with the leaf clip.

Index	Equation	Reference
NDVI (Normalized Difference Vegetation Index)	$\frac{R_{782}-R_{675}}{R_{782}+R_{675}}$	[54]
$NDVI_{750}$ (Red Edge Normalized Difference Vegetation Index)	$\frac{R_{750}-R_{705}}{R_{750}+R_{705}}$	[55]
SRI (Simple Ratio Index)	$\frac{R_{800}}{R_{680}}$	[56]
EVI (Enhanced Vegetation Index)	$\frac{2.5*R_{782}-R_{675}}{R_{782}+6*R_{675}-7.5*R_{445}+1}$	[57]
ARVI (Atmospherically resistant vegetation index)	$\frac{R_{865}-2*R_{660}+R_{470}}{R_{865}+2*R_{660}-R_{470}}$	[58]
SGI (Sum Green Index)	$Mean(R_{500}\|R_{600})$	[59]
mNDVI (modified Normalized Difference Vegetation Index)	$\frac{R_{752}-R_{702}}{R_{752}+R_{702}-2*R_{447}}$	[25]
mSR_{705} (modified Simple Ratio Index)	$\frac{R_{750}-R_{445}}{R_{705}-R_{445}}$	[25]
VOG1 (Vogelmann)	$\frac{R_{740}}{R_{720}}$	[60]
VOG2 (Vogelmann)	$\frac{R_{734}-R_{747}}{R_{715}+R_{726}}$	[60]
VOG3 (Vogelmann)	$\frac{R_{734}-R_{747}}{R_{715}+R_{720}}$	[60]
PRI (Photochemical Reflectance Index)	$\frac{R_{531}-R_{570}}{R_{531}+R_{570}}$	[61]
SIPI (Structure Insensitive Pigment Index)	$\frac{R_{800}-R_{445}}{R_{800}-R_{680}}$	[27]
RGI (Red Green Index)	$\frac{R_{690}}{R_{550}}$	[62]
PSRI (Plant Senescence Reflectance Index)	$\frac{R_{680}-R_{500}}{R_{750}}$	[26]
CRI1 (Carotenoid Reflectance Index)	$\frac{1}{R_{510}}-\frac{1}{R_{550}}$	[63]
CRI2 (Carotenoid Reflectance Index)	$\frac{1}{R_{510}}-\frac{1}{R_{700}}$	[63]
ARI2 (Anthocyanin Reflectance Index)	$R_{800}*\left(\frac{1}{R_{550}}-\frac{1}{R_{700}}\right)$	[64]
WBI (Water Band Index)	$\frac{R_{900}}{R_{970}}$	[65]
gNDVI (green Normalized Difference Vegetation Index)	$\frac{R_{872}-R_{559}}{R_{872}+R_{559}}$	[66]
PCAi-1	First component of PCA	–

3. Results

3.1. Sun and Shade Leaves Comparison

The light intensity within a dense *Phragmites* stand decreased exponentially (data not shown), resulting in significant illumination difference at the apical and basal parts of the plants, accounting for 1251 ± 245 µmol m^{-2} s^{-1} and 268 ± 88 µmol m^{-2} s^{-1} respectively (Mann–Whitney Rank Sum Test, $T = 6442$, $p \leq 0{,}001$). Prolonged exposure of leaves to different light intensities resulted in substantially different photophysiological parameters of the sun and shade leaves of *Phragmites* in dense reed

patches (Figures 2–4). As an effect of the lower irradiance, the I_k, ETR_{max}, Y(II) and qP of shade leaves decreased, while α and qN significantly increased (Figures 3 and 4).

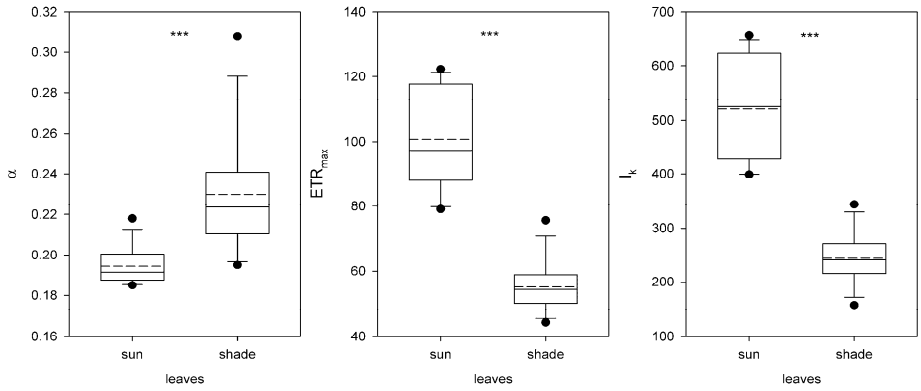

Figure 3. The maximum quantum yield for whole chain electron transport (α), the maximum electron transport capacity (ETR_{max}) and the theoretical light saturation intensity (I_k) for the sun and shade leaves of *Phragmites australis* in dense patches. Boxes encompass the 25% and 75% quartiles of all the data, the central solid and dashed lines represents the median and the average, bars extend to the 95% confidence limits, and dots represent outliers. For all bars $n = 15$. Differences were tested with the Mann-Whitney Rank Sum Test; *** indicates $p < 0.001$.

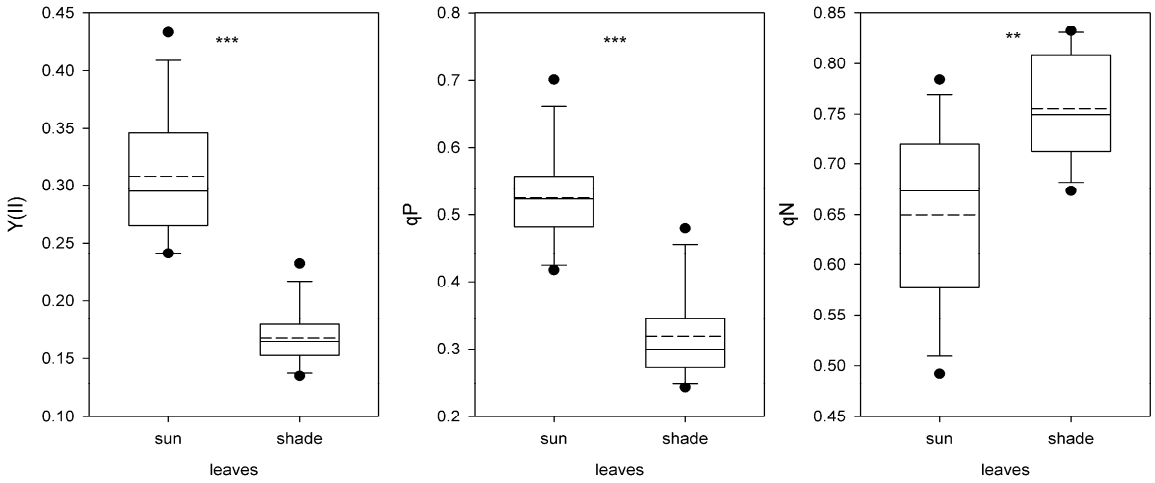

Figure 4. The quantum yield of PSII (Y(II)), photochemical (qP) and non-photochemical (qN) quenching for the sun and shade leaves of *Phragmites australis* in dense patches. Boxes encompass the 25% and 75% quartiles of all the data, the central solid and dashed lines represents the median and the average, bars extend to the 95% confidence limits, and dots represent outliers. For all bars $n = 15$. Differences were tested with the Mann–Whitney Rank Sum Test; ** indicates $p < 0.01$, while *** indicates $p < 0.001$.

These changes in photophysiological properties also appear on the reflectance of leaves affecting primarily the red-edge and the near-infrared (NIR) spectral regions. Figure 5 presents the leaf reflectance spectra between 400 nm and 1000 nm measured for sun and shade leaves of *Phragmites*. The reflectance in the NIR (700–1000 nm) spectrum for sun leaves was 6.5% higher compared to the shade leaves. The red edge inflection point shifted to a shorter wavelength from $\lambda_p = 713$ nm for the sun leaves to $\lambda_p = 701$ nm for the shade leaves.

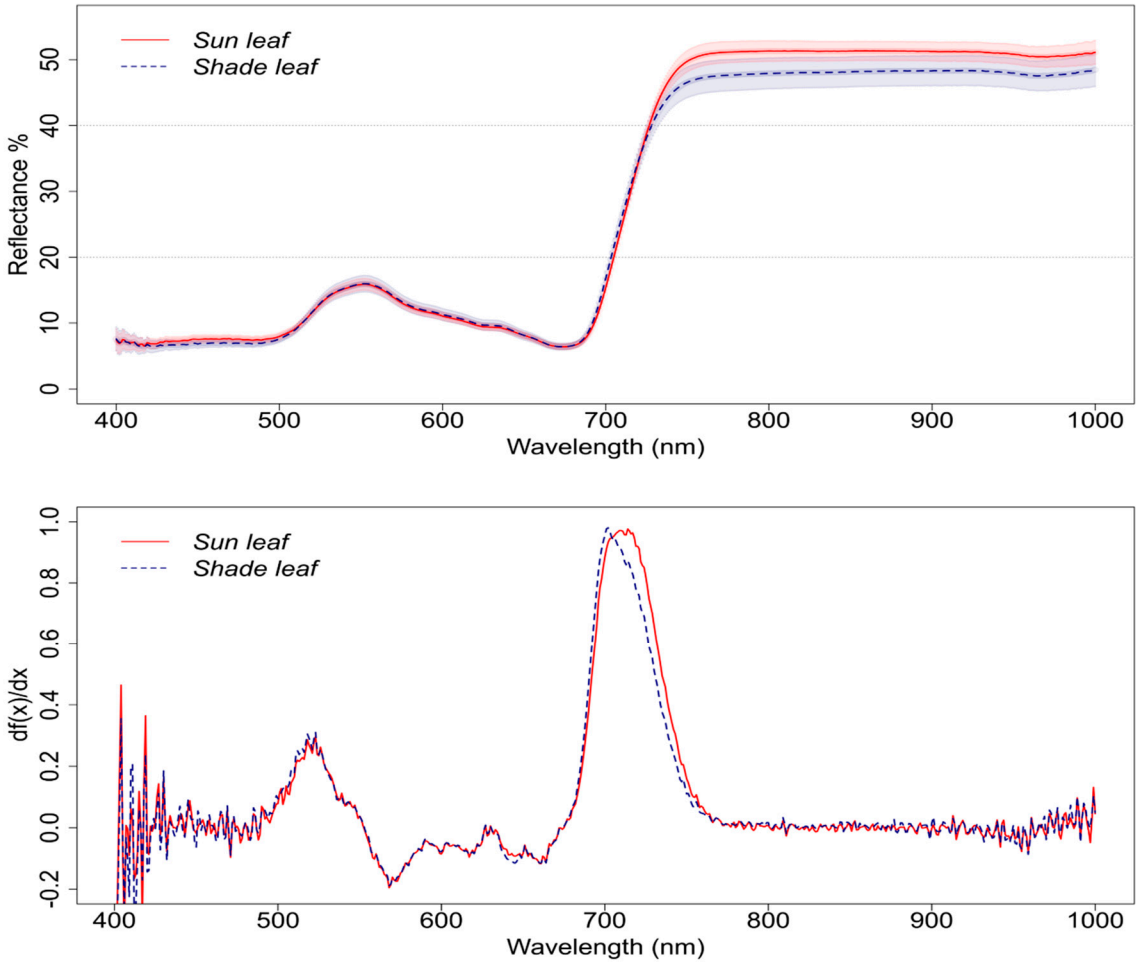

Figure 5. Mean (curve) and standard deviation (shaded area) of relative reflectance (ρ) of *Phragmites australis* sun (solid line) and shade (dashed line) leaves (upper inset) and the first derivative (lower inset). Each line is an average of 12 measurements.

The Principal Component Analysis (PCA) of the spectroradiometric data further revealed the difference between the reflectance of sun and shade leaves of *Phragmites* (Figure 6). The major diversity of the data is reflected in the NIR responses of the leaves, while the RGB component had no significant contribution in the explanation of the first two orthogonal principal components. The third and fourth principal components explained only the 2.6 and 1.5 of the variation inherited in the data, respectively, and were deemed insignificant and disregarded.

The R^2 graph resulting from the measurements during the two consecutive days of fieldwork cumulatively is presented in Figure 7. Values of R^2 corresponding to spectral pairs yielding $p > 0.05$ were deemed statistically insignificant and have been masked out of the graph for ease of interpretation. The graphs for parameters I_k and ETR_{max} were very similar (data not shown here), hence the graph of I_k has been disregarded for further analysis and is not presented.

Figure 8 presents the statistical results from the extraction of a few empirical vegetation indices, which were selected on the basis of differing statistical distribution between the shade and the sun leaves.

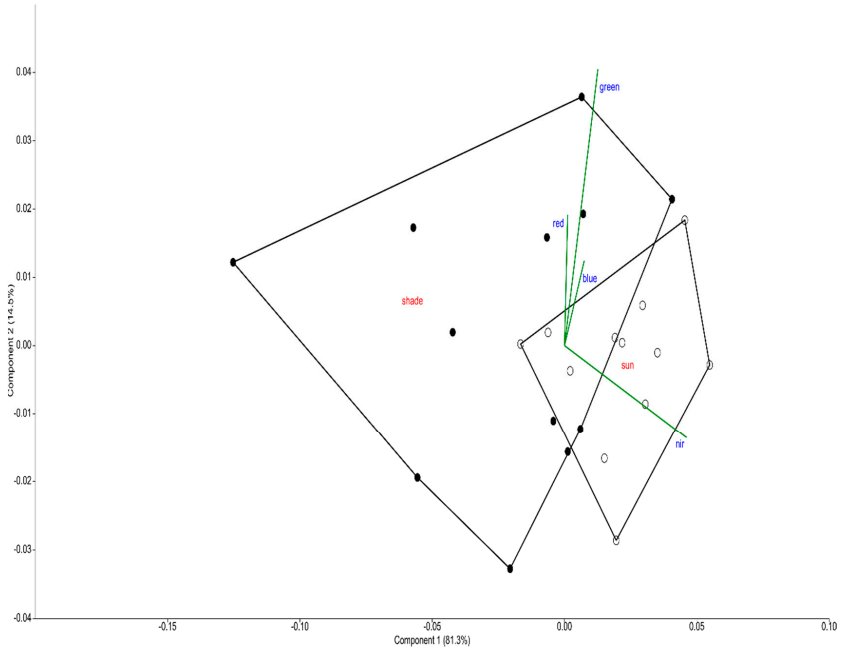

Figure 6. PCA of the spectral response features of sun (open circles) and shade (black circles) leaves of *Phragmites australis* in Lake Balaton. Axis 1 explains 81.3% of the variation, axis 2—14.5%.

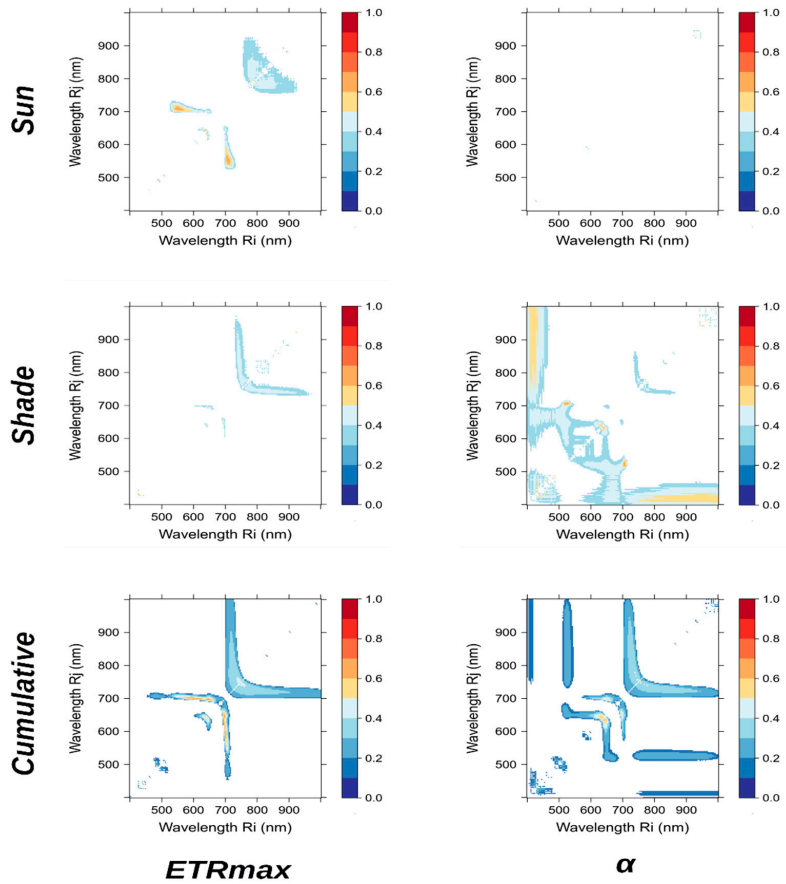

Figure 7. Coefficient of determination (R^2) between the two photophysiological parameters (ETRmax (left) and α (right)) and the NDSI (Ri, Rj) measured on *Phragmites australis* plants at Kerekedi Bay, Lake Balaton on 14–15 August. The NDSI was calculated using the exhaustive combinations of the hyperspectrum of reflectance of two wavebands at i and j. R^2 corresponding to spectral pairs yielding $p > 0.05$ (statistical insignificant) have been masked out (blank pixels).

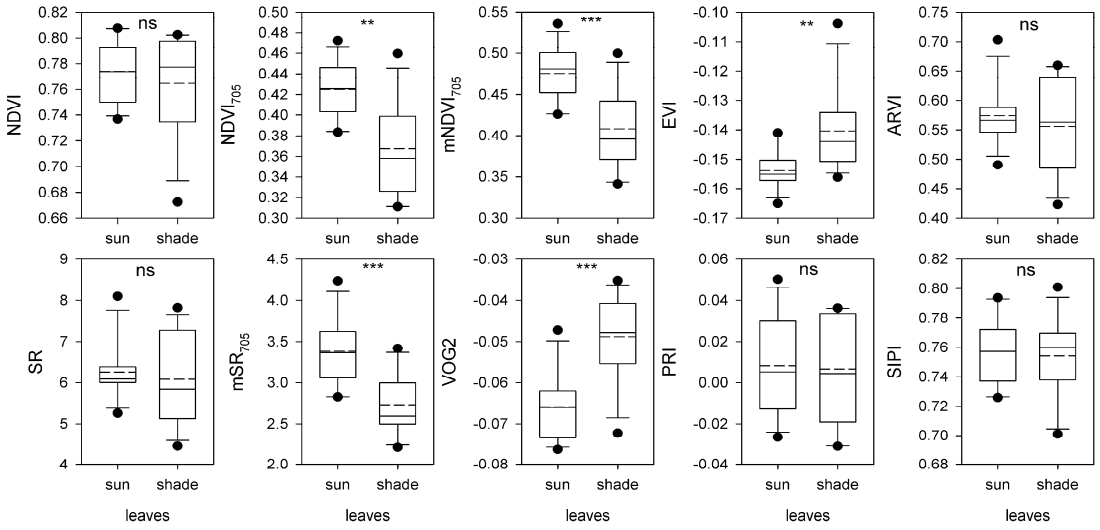

Figure 8. Boxplots of major vegetation indexes of sun and shade leaves of *Phragmites australis*. Data from different leaves were compared with Mann-Whitney Rank Sum Test: ns—Not significant, ** $p < 0.01$, *** $p < 0.001$.

3.2. Density Effect

In the second part of the experiment, the effect of the density of *Phragmites* stands on the photophysiological parameters and the reflectance of the oldest basal green leaves were studied. The majority of the photophysiological parameters (seven of nine) correlated with the density of plants (Table 3). Mostly negative correlations were determined (with increase in density the parameters were decreasing), although the different indices of the non-photochemical quenching positively correlated with the plant density. On the other hand, the majority of vegetation indices (13 of 21) showed no significant correlation (Table 3).

Table 3. Spearman rank order correlation between the density of the *Phragmites australis* patch and empirical vegetation indices and photophysiological data. $n = 24$, ns—Not significant, * $p < 0.05$, ** $p < 0.01$. In bold values the parameters for which the correlation is significant (i.e., $0 < p < 0.05$).

Vegetation Index	r^P
NDVI	−0.05 ^{ns}
$NDVI_{750}$	**−0.47 ***
SRI	−0.09 ^{ns}
EVI	0.36 ^{ns}
ARVI	−0.04 ^{ns}
SGI	0.04 ^{ns}
mNDVI	**−0.50 ***
mSR705	**−0.51 ***
VOG1	**−0.51 ***
VOG2	**0.56 ****
VOG3	**0.55 ****
PRI	−0.01 ^{ns}
SIPI	−0.05 ^{ns}
RGI	0.12 ^{ns}
PSRI	−0.07 ^{ns}
CRI1	0.08 ^{ns}
CRI2	0.31 ^{ns}
ARI2	**0.50 ***
WBI	−0.22 ^{ns}
gNDVI	−0.19 ^{ns}
PCAi-1	**0.59 ****

Table 3. *Cont.*

Photophysiological parameter	r^P
α	**0.51** *
ETR_{max}	**−0.56** **
I_k	**−0.58** **
F	0.26 ^{ns}
F_m'	−0.11 ^{ns}
Y(II)	**−0.56** **
qN	**0.58** **
qP	**−0.54** **
ETR	**−0.56** **

4. Discussion

Due to its high adaptability, high growth rate and predominantly clonal vegetative reproduction, *Phragmites* monopolized littoral zones of most freshwater lakes and became the dominant species [40,67–69]. As seed dispersal in *Phragmites* stands is impossible in water covered areas, the spatial distribution of their shoots (ramets) is mainly determined by vegetative (clonal) spread using rhizomes. Clonal *Phragmites* is physiologically integrated within the genets (clones) facilitating cooperation [70–72] and, thus, substantially changing our perception of competition within a reed stand. In the end, the interconnected clone is the basic physiological unit that interacts with its environment [70–72]. The density of *Phragmites* plants within the stand is affected by two counteracting processes: the plants tend to remain as dense as the rhizome architecture and the habitat's resource-supplying capacity allows, while the density of plants is limited, among others, by optical properties within the stand [69,73]. Respectively, the density of *Phragmites* affects the optical environment of the stands: the denser the stand, the less light reaches the basal parts of the plants.

In this study performed in a temperate zone freshwater lake, *Phragmites* exhibited major differences between apical (sun) and basal (shade) leaves. Our results (Figures 2–4) show that reed in dense stands could vertically alleviate irradiance, so that while the apical part of plants exposed to sun could develop sun adapted leaves, the fully shaded conditions at the basal part result in shade-tolerant adaptations of *Phragmites*. All the determined changes showed adaptations to specific light intensities of the apical and basal part of *Phragmites*: electron transport rates (proxy of photosynthetic activity), photochemical quenching and theoretical light saturation intensities of the sun leaves were 84%, 63% and 113% higher than in shade leaves showing that leaves were adapted to utilise higher light intensities. On the other hand, the shade-tolerant leaves were able to react better to smallest changes in light environment (21% higher quantum yield for whole chain electron transport) and maintain alternative metabolic pathways (17% higher nonphotochemical quenching). Moreover, the results indicate that the shade leaves inherit more variability in their spectral profile (standard deviation in Figure 5 and the PCs in Figure 6), and are thus potentially able to absorb larger spectral variety as compared to sun leaves. These adaptations were consistent and were translated to foliar reflectance data. Similar changes in the vertical profile of vegetation have been observed in other studies; for instance, D'Odorico et al. [74], when studying the leaf photosynthetic traits for top and bottom canopy leaves for winter barley (*Hordeum vulgare* L.) and rape seed (*Brassica napus* L.), found that traits such as the maximum photosynthetic capacity, dark respiration, leaf nitrogen and chlorophyll contents and leaf mass per area presented consistently higher values for top leaves throughout the growing season and for both crop types.

A closer look at the reflectance curves of sun and shade leaves (Figure 5) presents that the red-edge shift observed, from λ_p = 713 nm for the sun leaves to λ_p = 701 nm for the shade leaves, is affecting the vegetation indices, and especially the ones that use this part of the spectrum, such as the VOG2 and the mNDVI which demonstrate the highest correlation amongst the empirical vegetation indices (Table 2). A similar slight change is observed in the the NIR reflectance (700–1000 nm) spectrum for which sun leaves demonstrated 6.5% higher reflectance compared to the shade leaves; however, these

both changes are comparatively small and as the standard deviation indicates in Figure 5, they might be attributed to variability within the data. Similar studies have presented contrasting results; in an older study, Schultz [9] reports that leaf reflectance was independent of the sun-shade environment of the samples within the canopy, regardless of the leaf age and the acquisition time during the season; however his samples were grapevine (*Vitis vinifera* L.) leaves grown under commercial practice, which normally are not grown in as a dense environment as *Phragmites*. An earlier study, however, from Gausman [10] suggest that there are considerable differences in the visible reflectance of the upper surface of the Valencia orange tree leaves.

While the reflectance curves (Figure 5) present the spectral differences of the two experimental sample groups, Figure 7 presents the association between the full combination of derived spectral NDSI indices and the physiological parameters ETR_{max} and α. An observation arising from the results is that the red-edge region is the strongest associated with ETR_{max} for the sun leaves and the cumulative measurements; this is not so apparent in the shade leaves graph, perhaps because the physiological variability (as indicated by the standard deviation) of the shade leaves is smaller (Figure 3) and consequently the correlation weaker. Just above 700 nm there is a spectral area in the sun leaves for ETR_{max} with a correlation of $R^2 > 0.60$ (maximum $R^2 = 0.65$ at wavelength combination 708/558); this area coincides with the inflection point of the sun leaves (i.e., $\lambda_p = 713$ nm) (Figure 5) which indicates the importance of the inflection point in regard to ETR_{max}. In the cumulative graph of ETR_{max} the same highest correlation is encountered in the same spectral area in a slightly narrower but wider window; the narrow-band pair with the highest correlation is at 696/651 with $R^2 = 0.65$. In the graph of ETR_{max} for the shade leaves there is no correlation with $R^2 > 0.5$. In regard to α, the opposite from the ETR_{max} is observed; the statistical distribution for the shade leaves has a larger standard deviation and an outlier is apparent (Figure 3). The graph for the sun leaves and α do not present statistically significant results, however, the graph for the shade leaves presents two areas of interest; first, there is a narrow isolated spectral combination at 708/525 with $R^2 = 0.68$ which is the highest correlation coefficient we have found in this study; this fact seconds the importance of the inflection point for the shade leaves ($\lambda_p = 701$ nm) which falls within this area and is 7 nm apart from the spectral combination with the maximum R^2. Secondly, there is a wider spectral region constructed at the very short visible and the very long near-infrared wavelengths of the available spectrum, which provides $R^2 > 0.5$. The cumulative graph for α indicates a narrow area at 636/642 with a correlation of $R^2 = 0.61$ which is also evidenced in the shade leaves graph.

It is worth noting that, in order to collect the chlorophyll fluorescence measurements, a 20 min adaptation period is required for each sample; this fact in combination with the requirement to record the data around solar noon (which was between 10:00 am and 13:00 pm local time) restricts the number of measurements that can actually be recorded within this time period from a single PAM device, and consequently results to a low repeat count in the experimental set up for a single day; this was the reason that we used cumulatively the data collected during two consecutive days as presented above. Moreover, we attempted to analyse the data separately for these two days; the differences in this case were large (results not shown here) and we believe that the main reason is the small sample size for a single individual day. Second, environmental (e.g., temperature) and vegetative (e.g., density, heterogeneity) conditions change even between consecutive days and we only report the similarities in the clear sky conditions, which is just one of the many variables that can affect the physiological and spectral behaviour of plants.

Figure 8 presents the results from selected spectral indices indicating which ones are sensitive and insensitive to shade and sun leaves; this can provide information in estimating the ratio of sun and shade leaves from the canopy. It is apparent that the spectral indices $NDVI_{705}$, mNDVI, EVI, mSR_{705}, VOG2 provide distinguishing results for sun and shade leaves, while the spectral indices NDVI, ARVI, SR, PRI, SIPI do not demonstrate any important differences for sun and shade leaves in their respective statistical distribution. It is worth noting the considerably different results from NDVI and $NDVI_{705}$; the former results to almost identical distributions for sun and shade leaves while the latter provides

distinguishing results; this is an indication that narrow-band indices highly depend on the wavelength used and are not to be assumed identical with the broadband indices and generalized. Moreover, PRI, which is a spectral index assumed to be related to photochemistry, did not yield any significant differences for the two leaf sets.

Our study relied on spectroscopic data and the spectral results indicate narrow-bands of correlation with the photophysiological parameters. In the context of wetlands, several studies have been utilizing such data, as for instance, Pengra et al. [75] used EO-1 Hyperion hyperspectral sensor to map the extent and location of invasive monodominant *Phragmites* in Green Bay, WI, USA. with 81.4% accuracy. These type of satellite hyperspectral data could be used, based on the findings of our study, to investigate the density and physiological status of *Phragmites* based on the proposed narrow-band NDSI spectral indices. Nevertheless, care should be taken when translating our findings, which are based on foliar data, to satellite or airborne imagery which observes foliar data; in this case, a radiative transfer model could be used to bridge the gap from leaf to canopy level.

Nevertheless, wetland characteristics are mapped with remote sensing based mainly on multispectral data from a variety of platforms, such as unmanned aerial vehicles (UAVs) (e.g., [76–79]), or satellite passive sensors, such as the Landsat Thematic Mapper (TM) and Indian Remote Sensing Satellite (IRS) [80], Satellite pour l'Observation de la Terre (SPOT) [81], WorldView-2 [82] and Sentinel-2 [83]). Figure 7 indicates that there are only a few broadband spectral regions correlating with the parameters under study, and specifically the reflectance of the shade leaves with α at the shorter wavelengths. However, as more of these satellites integrate narrow-band spectral channels in their capabilities (e.g., Sentinel-2, WorldView 2/3, RapidEye) it would be possible to utilize the findings of our results in regard to ETR and α, since we suggest that the red-edge is the most important spectral region, and this is the available spectral region that the narrow-band channels onboard satellites currently integrate.

5. Conclusions

This study examined the intertwined effect of plant density and sun/shade leaves' photophysiology in regard to chlorophyll fluorescence and hyperspectral response. Although *Phragmites* is considered a sun adapted species, in our study we showed that basal parts of the plant exhibited a shade-tolerant nature in photophysiological response to foliage shading. Low irradiance increased the acclimation of plants to low light conditions. At normal conditions and at high plant densities only the signals from sun leaves could reach from the canopy level, although even the slightest move of canopy (breeze, wind) could expose the basal, shade leaves affecting the acquired high resolution (not satellite) data. At relatively lower densities within the stand the vertical light attenuation was still large, and this modified the photophysiology of basal foliage, so *Phragmites* exhibit signals from both sun and shade leaves, thus showing higher variability at the data level of canopy reflectance. At low densities, the vertical light attenuation is low, making all the leaves exhibit dominantly sun-adopted properties. The hyperspectral response from the sun and shade leaves has been found to differ and the charts of the coefficient of determination indicate that there are specific narrow-band spectral regions associated to the leaf vertical position and the photophysiological parameter under study. The spectral bands around the red-edge inflection point for each case of sun and shade leaves has been found to correlate strongly with ETR_{max} and α. When analyzing the data cumulatively, independent of their vertical position within the stand, we found correlations of $R^2 = 0.65$ (696/651) and $R^2 = 0.61$ (636/642) for the ETR_{max} and α, respectively. The outcomes of this study could help to predict density of reed stands or correct previously seen anomalies.

Author Contributions: D.S. and V.R.T. collected the data and wrote the paper. V.R.T. analyzed the chlorophyll fluorescence data and D.S. analyzed the hyperspectral data. All authors have read and agreed to the published version of the manuscript.

Funding: This research was funded by GIONET, supported by the European Commission, Marie Curie Programme, Initial Training Networks, grant agreement number PITN-GA-2010-264509. This study was funded by grant from the Hungarian National Research, Development and Innovation Office NKFIH KH-129505.

Acknowledgments: The authors would like to thank the financial support from GIONET, during which the field data collection was carried out.

Conflicts of Interest: The authors declare no conflict of interest.

References

1. Lacoul, P.; Freedman, B. Environmental influences on aquatic plants in freshwater ecosystems. *Environ. Rev.* **2006**, *14*, 89–136. [CrossRef]
2. Mooney, H.A.; Ehleringer, J.R. Photosynthesis. In *Plant Ecology*; Blackwell Publishing Ltd.: Oxford, UK, 2009; pp. 1–27. ISBN 978-1-4443-1364-2.
3. Tilman, D. Mechanisms of Plant Competition. In *Plant Ecology*; Blackwell Publishing Ltd.: Oxford, UK, 2009; pp. 239–261. ISBN 978-1-4443-1364-2.
4. Lichtenthaler, H.K.; Buschmann, C.; Döll, M.; Fietz, H.J.; Bach, T.; Kozel, U.; Rahmsdorf, U. Photosynthetic activity, chloroplast ultrastructure, and leaf characteristics of high-light and low-light plants and of sun and shade leaves. *Photosynth. Res.* **1981**, *2*, 115–141. [CrossRef]
5. Givnish, T.J. Adaptation to sun and shade: A whole-plant perspective. *Funct. Plant Biol.* **1988**, *15*, 63–92. [CrossRef]
6. Boardman, N.T. Comparative photosynthesis of sun and shade plants. *Annu. Rev. Plant Physiol.* **1977**, *28*, 355–377. [CrossRef]
7. Crawley, M.J. Life History and Environment. In *Plant Ecology*; Blackwell Publishing Ltd.: Oxford, UK, 2009; pp. 73–131. ISBN 978-1-4443-1364-2.
8. Lichtenthaler, H.K.; Ač, A.; Marek, M.V.; Kalina, J.; Urban, O. Differences in pigment composition, photosynthetic rates and chlorophyll fluorescence images of sun and shade leaves of four tree species. *Plant Physiol. Biochem.* **2007**, *45*, 577–588. [CrossRef] [PubMed]
9. Schultz, H.R. Leaf absorptance of visible radiation in Vitis vinifera L.: Estimates of age and shade effects with a simple field method. *Sci. Hortic.* **1996**, *66*, 93–102. [CrossRef]
10. Gausman, H.W. Evaluation of factors causing reflectance differences between sun and shade leaves. *Remote Sens. Environ.* **1984**, *15*, 177–181. [CrossRef]
11. Mathur, S.; Jain, L.; Jajoo, A. Photosynthetic efficiency in sun and shade plants. *Photosynthetica* **2018**, *56*, 354–365. [CrossRef]
12. Haslam, S.M. The development of shoots in Phragmites communis Trin. *Ann. Bot.* **1969**, *33*, 695–709. [CrossRef]
13. Tucker, G.C. The Genera of Arundinoideae (Gramineae) in the Southeastern United States. *J. Arnold Arbor.* **1990**, *71*, 145–177. [CrossRef]
14. Brix, H. The European research project on reed die-back and progression (EUREED). *Limnologica* **1999**, *29*, 5–10. [CrossRef]
15. Van der Putten, W.H. Die-back of Phragmites australis in European wetlands: An overview of the European research programme on reed die-back and progression (1993–1994). *Aquat. Bot.* **1997**, *59*, 263–275. [CrossRef]
16. Ostendorp, W. 'Die-back' of reeds in Europe—A critical review of literature. *Aquat. Bot.* **1989**, *35*, 5–26. [CrossRef]
17. Fogli, S.; Marchesini, R.; Gerdol, R. Reed (Phragmites australis) decline in a brackish wetland in Italy. *Mar. Environ. Res.* **2002**, *53*, 465–479. [CrossRef]
18. Genty, B.; Briantais, J.M.; Baker, N.R. The relationship between the quantum yield of photosynthetic electron transport and quenching of chlorophyll fluorescence. *Biochim. Biophys. Acta (BBA)-Gen. Subj.* **1989**, *990*, 87–92. [CrossRef]
19. Krause, G.H.; Weis, E. Chlorophyll fluorescence and photosynthesis: The basics. *Annu. Rev. Plant Biol.* **1991**, *42*, 313–349. [CrossRef]
20. Bąba, W.; Kompała-Bąba, A.; Zabochnicka-Świątek, M.; Luźniak, J.; Hanczaruk, R.; Adamski, A.; Kalaji, H. Discovering trends in photosynthesis using modern analytical tools: More than 100 reasons to use chlorophyll fluorescence. *Photosynthetica* **2019**, *57*, 668–679. [CrossRef]

21. Kwok, R. Ecology's remote-sensing revolution. *Nature* **2018**, *556*, 137–139. [CrossRef]
22. Stratoulias, D.; Balzter, H.; Zlinszky, A.; Tóth, V.R. Assessment of ecophysiology of lake shore reed vegetation based on chlorophyll fluorescence, field spectroscopy and hyperspectral airborne imagery. *Remote Sens. Environ.* **2015**, *157*, 72–84. [CrossRef]
23. Zarco-Tejada, P.J.; Miller, J.R.; Noland, T.L.; Mohammed, G.H.; Sampson, P.H. Scaling-up and model inversion methods with narrowband optical indices for chlorophyll content estimation in closed forest canopies with hyperspectral data. *IEEE Trans. Geosci. Remote Sens.* **2001**, *39*, 1491–1507. [CrossRef]
24. Gitelson, A.A.; Merzlyak, M.N. Signature analysis of leaf reflectance spectra: Algorithm development for remote sensing of chlorophyll. *J. Plant Physiol.* **1996**, *148*, 494–500. [CrossRef]
25. Sims, D.A.; Gamon, J.A. Relationships between leaf pigment content and spectral reflectance across a wide range of species, leaf structures and developmental stages. *Remote Sens. Environ.* **2002**, *81*, 337–354. [CrossRef]
26. Merzlyak, M.N.; Gitelson, A.A.; Chivkunova, O.B.; Rakitin, V.Y. Non-destructive optical detection of pigment changes during leaf senescence and fruit ripening. *Physiol. Plant.* **1999**, *106*, 135–141. [CrossRef]
27. Peñuelas, J.; Filella, I.; Gamon, J.A. Assessment of photosynthetic radiation-use efficiency with spectral reflectance. *New Phytol.* **1995**, *131*, 291–296. [CrossRef]
28. Gamon, J.A.; Penuelas, J.; Field, C.B. A narrow-waveband spectral index that tracks diurnal changes in photosynthetic efficiency. *Remote Sens. Environ.* **1992**, *41*, 35–44. [CrossRef]
29. Pieczywek, P.M.; Cybulska, J.; Szymańska-Chargot, M.; Siedliska, A.; Zdunek, A.; Nosalewicz, A.; Kurenda, A. Early detection of fungal infection of stored apple fruit with optical sensors–Comparison of biospeckle, hyperspectral imaging and chlorophyll fluorescence. *Food Control* **2018**, *85*, 327–338. [CrossRef]
30. Tan, C.W.; Wang, D.L.; Zhou, J.; Du, Y.; Luo, M.; Zhang, Y.J.; Guo, W.S. Assessment of F v/F m absorbed by wheat canopies employing in-situ hyperspectral vegetation indexes. *Sci. Rep.* **2018**, *8*, 9525. [CrossRef] [PubMed]
31. Zarco-Tejada, P.J.; González-Dugo, M.V.; Fereres, E. Seasonal stability of chlorophyll fluorescence quantified from airborne hyperspectral imagery as an indicator of net photosynthesis in the context of precision agriculture. *Remote Sens. Environ.* **2016**, *179*, 89–103. [CrossRef]
32. Wolanin, A.; Rozanov, V.V.; Dinter, T.; Noël, S.; Vountas, M.; Burrows, J.P.; Bracher, A. Global retrieval of marine and terrestrial chlorophyll fluorescence at its red peak using hyperspectral top of atmosphere radiance measurements: Feasibility study and first results. *Remote Sens. Environ.* **2015**, *166*, 243–261. [CrossRef]
33. Joiner, J.; Yoshida, Y.; Guanter, L.; Middleton, E.M. New methods for the retrieval of chlorophyll red fluorescence from hyperspectral satellite instruments: Simulations and application to GOME-2 and SCIAMACHY. *Atmos. Meas. Tech.* **2016**, *9*, 3939–3967. [CrossRef]
34. Peñuelas, J.; Baret, F.; Filella, I. Semi-empirical indices to assess carotenoids/chlorophyll a ratio from leaf spectral reflectance. *Photosynthetica* **1995**, *31*, 221–230.
35. Zhang, C.; Filella, I.; Garbulsky, M.; Peñuelas, J. Affecting factors and recent improvements of the photochemical reflectance index (PRI) for remotely sensing foliar, canopy and ecosystemic radiation-use efficiencies. *Remote Sens.* **2016**, *8*, 677. [CrossRef]
36. Wong, C.Y.; Gamon, J.A. Three causes of variation in the photochemical reflectance index (PRI) in evergreen conifers. *New Phytol.* **2015**, *206*, 187–195. [CrossRef] [PubMed]
37. Gamon, J.A.; Field, C.B.; Goulden, M.L.; Griffin, K.L.; Hartley, A.E.; Joel, G.; Valentini, R. Relationships between NDVI, canopy structure, and photosynthesis in three Californian vegetation types. *Ecol. Appl.* **1995**, *5*, 28–41. [CrossRef]
38. Grace, J.; Nichol, C.; Disney, M.; Lewis, P.; Quaife, T.; Bowyer, P. Can we measure terrestrial photosynthesis from space directly, using spectral reflectance and fluorescence? *Glob. Chang. Biol.* **2007**, *13*, 1484–1497. [CrossRef]
39. Dechant, B.; Cuntz, M.; Vohland, M.; Schulz, E.; Doktor, D. Estimation of photosynthesis traits from leaf reflectance spectra: Correlation to nitrogen content as the dominant mechanism. *Remote Sens. Environ.* **2017**, *196*, 279–292. [CrossRef]
40. Tóth, V.R. Reed stands during different water level periods: Physico-chemical properties of the sediment and growth of Phragmites australis of Lake Balaton. *Hydrobiologia* **2016**, *778*, 193–207. [CrossRef]

41. Tóth, V.R.; Szabó, K. Morphometric structural analysis of Phragmites australis stands in Lake Balaton. In *Annales de Limnologie-International Journal of Limnology*; EDP Sciences: Nantes, France, 2012; Volume 48, pp. 241–251.
42. Zlinszky, A.; Mücke, W.; Lehner, H.; Briese, C.; Pfeifer, N. Categorizing wetland vegetation by airborne laser scanning on Lake Balaton and Kis-Balaton, Hungary. *Remote Sens.* **2012**, *4*, 1617–1650. [CrossRef]
43. Stratoulias, D. Assessment of physiological status and spatial distribution of emergent macrophytes based on imaging spectroscopy (Doctoral dissertation, Department of Geography). *Dep. Geogr.* **2015**.
44. Stratoulias, D.; Balzter, H.; Sykioti, O.; Zlinszky, A.; Tóth, V. Evaluating Sentinel-2 for lakeshore habitat mapping based on airborne hyperspectral data. *Sensors* **2015**, *15*, 22956–22969. [CrossRef]
45. Villa, P.; Pinardi, M.; Tóth, V.R.; Hunter, P.D.; Bolpagni, R.; Bresciani, M. Remote sensing of macrophyte morphological traits: Implications for the management of shallow lakes. *J. Limnol.* **2017**. [CrossRef]
46. Stratoulias, D.; Keramitsoglou, I.; Burai, P.; Csaba, L.; Zlinszky, A.; Tóth, V.R.; Balzter, H. A framework for lakeshore vegetation assessment using field spectroscopy and airborne hyperspectral imagery. *Earth Obs. Land Emerg. Monit.* **2017**, *159*. [CrossRef]
47. Stratoulias, D.; Balzter, H.; Zlinszky, A.; Tóth, V.R. A comparison of airborne hyperspectral-based classifications of emergent wetland vegetation at Lake Balaton, Hungary. *Int. J. Remote Sens.* **2018**, *39*, 5689–5715. [CrossRef]
48. Wilkie, C.J.; Scott, E.M.; Miller, C.; Tyler, A.N.; Hunter, P.D.; Spyrakos, E. Data fusion of remote-sensing and in-lake chlorophylla data using statistical downscaling. *Procedia Environ. Sci.* **2015**, *26*, 123–126. [CrossRef]
49. Blix, K.; Pálffy, K.; RTóth, V.; Eltoft, T. Remote Sensing of Water Quality Parameters over Lake Balaton by Using Sentinel-3 OLCI. *Water* **2018**, *10*, 1428. [CrossRef]
50. Eilers, P.H.C.; Peeters, J.C.H. A model for the relationship between light intensity and the rate of photosynthesis in phytoplankton. *Ecol. Model.* **1988**, *42*, 199–215. [CrossRef]
51. R Core Team. R: A language and environment for statistical computing. *Computing* **2013**. [CrossRef]
52. Stagakis, S.; Markos, N.; Sykioti, O.; Kyparissis, A. Monitoring canopy biophysical and biochemical parameters in ecosystem scale using satellite hyperspectral imagery: An application on a Phlomis fruticosa Mediterranean ecosystem using multiangular CHRIS/PROBA observations. *Remote Sens. Environ.* **2010**, *114*, 977–994. [CrossRef]
53. Inoue, Y.; Sakaiya, E.; Zhu, Y.; Takahashi, W. Diagnostic mapping of canopy nitrogen content in rice based on hyperspectral measurements. *Remote Sens. Environ.* **2012**, *126*, 210–221. [CrossRef]
54. Tucker, C.J. Red and photographic infrared linear combinations for monitoring vegetation. *Remote Sens. Environ.* **1979**, *8*, 127–150. [CrossRef]
55. Gitelson, A.A.; Merzlyak, M.N. Spectral reflectance changes associated with autumn senescence of Aesculus hippocastanum L. and Acer platanoides L. leaves. Spectral features and relation to chlorophyll estimation. *J. Plant Physiol.* **1994**, *143*, 286–292. [CrossRef]
56. Jordan, C.F. Derivation of leaf area index from quality of light on the forest floor. *Ecology* **1969**, *50*, 663–666. [CrossRef]
57. Huete, A.; Didan, K.; Miura, T.; Rodriguez, E.P.; Gao, X.; Ferreira, L.G. Overview of the radiometric and biophysical performance of the MODIS vegetation indices. *Remote Sens. Environ.* **2002**, *83*, 195–213. [CrossRef]
58. Kaufman, Y.J.; Tanre, D. Atmospherically resistant vegetation index (ARVI) for EOS-MODIS. *IEEE Trans. Geosci. Remote Sens.* **1992**, *30*, 261–270. [CrossRef]
59. Gamon, J.A.; Surfus, J. Assessing leaf pigment content and activity with a reflectometer. *New Phytol.* **1999**, *143*, 105–117. [CrossRef]
60. Vogelmann, J.E.; Rock, B.N.; Moss, D.M. Red edge spectral measurements from sugar maple leaves. *Int. J. Remote Sens.* **1993**, *14*, 1563–1575. [CrossRef]
61. Gamon, J.A.; Serrano, L.; Surfus, J.S. The photochemical reflectance index: An optical indicator of photosynthetic radiation use efficiency across species, functional types and nutrient levels. *Oecologia* **1997**, *112*, 492–501. [CrossRef]
62. Zarco-Tejada, P.J.; Berjón, A.; López-Lozano, R.; Miller, J.R.; Martín, P.; Cachorro, V.; González, M.R.; de Frutos, A. Assessing vineyard condition with hyperspectral indices: Leaf and canopy reflectance simulation in a row-structured discontinuous canopy. *Remote Sens. Environ.* **2005**, *99*, 271–287. [CrossRef]

63. Gitelson, A.A.; Zur, Y.; Chivkunova, O.B.; Merzlyak, M.N. Assessing carotenoid content in plant leaves with reflectance spectroscopy. *Photochem. Photobiol.* **2002**, *75*, 272–281. [CrossRef]
64. Gitelson, A.A.; Merzlyak, M.N.; Chivkunova, O.B. Optical properties and nondestructive estimation of anthocyanin content in plant leaves. *Photochem. Photobiol.* **2001**, *71*, 38–45. [CrossRef]
65. Peñuelas, J.; Filella, I.; Biel, C.; Serrano, L.; Save, R. The reflectance at the 950–970 nm region as an indicator of plant water status. *Int. J. Remote Sens.* **1993**, *14*, 1887–1905. [CrossRef]
66. Gitelson, A.A.; Merzlyak, M.N. Remote sensing of chlorophyll concentration in higher plant leaves. *Adv. Space Res.* **1998**, *22*, 689–692. [CrossRef]
67. Clevering, O.A. An investigation into the effects of nitrogen on growth and morphology of stable and die-back populations of Phragmites australis. *Aquat. Bot.* **1998**, *60*, 11–25. [CrossRef]
68. Kühl, H.; Koppitz, H.; Rolletschek, H.; Kohl, J.G. Clone specific differences in a Phragmites australis stand: I. Morphology, genetics and site description. *Aquat. Bot.* **1999**, *64*, 235–246. [CrossRef]
69. Vretare, V.; Weisner, S.E.; Strand, J.A.; Granéli, W. Phenotypic plasticity in Phragmites australis as a functional response to water depth. *Aquat. Bot.* **2001**, *69*, 127–145. [CrossRef]
70. Pitelka, L.F.; Ashmun, L.W. Physiology and integration of ramets in clonal plants. In *Population Biology and Evolution of Clonal Organisms*; Yale University Press: New Haven, CT, USA, 1985; ISBN 0-300-03650-7.
71. Hara, T.; Van der Toorn, J.; Mook, J.H. Growth dynamics and size structure of shoots of Phragmites australis, a clonal plant. *J. Ecol.* **1993**, *81*, 47–60. [CrossRef]
72. Amsberry, L.; Baker, M.A.; Ewanchuk, P.J.; Bertness, M.D. Clonal integration and the expansion of Phragmites australis. *Ecol. Appl.* **2000**, *10*, 1110–1118. [CrossRef]
73. Santamaría, L. Why are most aquatic plants widely distributed? Dispersal, clonal growth and small-scale heterogeneity in a stressful environment. *Acta Oecol.* **2002**, *23*, 137–154. [CrossRef]
74. D'Odorico, P.; Emmel, C.; Revill, A.; Liebisch, F.; Eugster, W.; Buchmann, N. Vertical patterns of photosynthesis and related leaf traits in two contrasting agricultural crops. *Funct. Plant Biol.* **2019**, *46*, 213–227. [CrossRef]
75. Pengra, B.W.; Johnston, C.A.; Loveland, T.R. Mapping an invasive plant, Phragmites australis, in coastal wetlands using the EO-1 Hyperion hyperspectral sensor. *Remote Sens. Environ.* **2007**, *108*, 74–81. [CrossRef]
76. Boon, M.A.; Greenfield, R.; Tesfamichael, S. Wetland assessment using unmanned aerial vehicle (UAV) photogrammetry. *ISPRS Ann. Photogramm. Remote Sens. Spat. Inf. Sci.* **2016**, *41*, 781–788. [CrossRef]
77. Samiappan, S.; Turnage, G.; Hathcock, L.; Casagrande, L.; Stinson, P.; Moorhead, R. Using unmanned aerial vehicles for high-resolution remote sensing to map invasive Phragmites australis in coastal wetlands. *Int. J. Remote Sens.* **2017**, *38*, 2199–2217. [CrossRef]
78. Pande-Chhetri, R.; Abd-Elrahman, A.; Liu, T.; Morton, J.; Wilhelm, V.L. Object-based classification of wetland vegetation using very high-resolution unmanned air system imagery. *Eur. J. Remote Sens.* **2017**, *50*, 564–576. [CrossRef]
79. Tóth, V.R. Monitoring spatial variability and temporal dynamics of Phragmites using unmanned aerial vehicles. *Front. Plant Sci.* **2018**, *9*, 728. [CrossRef] [PubMed]
80. Arzandeh, S.; Wang, J. Monitoring the change of Phragmites distribution using satellite data. *Can. J. Remote Sens.* **2003**, *29*, 24–35. [CrossRef]
81. Poulin, B.; Davranche, A.; Lefebvre, G. Ecological assessment of Phragmites australis wetlands using multi-season SPOT-5 scenes. *Remote Sens. Environ.* **2010**, *114*, 1602–1609. [CrossRef]
82. Mutanga, O.; Adam, E.; Cho, M.A. High density biomass estimation for wetland vegetation using WorldView-2 imagery and random forest regression algorithm. *Int. J. Appl. Earth Obs. Geoinf.* **2012**, *18*, 399–406. [CrossRef]
83. Kaplan, G.; Avdan, U. Mapping and monitoring wetlands using Sentinel-2 satellite imagery. *ISPRS Ann. Photogramm. Remote Sens. Spat. Inf. Sci.* **2017**, *4*, 271–277. [CrossRef]